Supporting Information

Electronic Structure Regulation Promotes tandem Electrochemical Nitrate Reduction on Cu modified porous CoO nanosheets

Yuanyuan Yang, [#a] *Fuhao Qi,* [#a] *Xiaolu Liu,* [a] *Yangzheng Zhao,* [a] *Jingxiang Xu,* [a] *and Huan Wang**[a]

[a]College of Chemistry, Chemical Engineering and Materials Science, Shandong Normal University, Jinan 250014, China

*Corresponding author. E-mail: huanwang@sdnu.edu.cn

[#]Y. Y. Yang and F. H. Qi contributed equally.

Supporting Experimental Section

Chemicals. Nafion (5 wt%) and maleic acid ($C_4H_4O_4$, ≥ 99.0%) were obtained from Sigma−Aldrich. Hydrochloric acid (HCl, ~36.0−38.0 wt%), cobalt (II) nitrate hexahydrate ($Co(NO_3)_2·6H_2O$, > 98.5%), copper (II) nitrate trihydrate ($Cu(NO_3)_2·3H_2O$, 99~102%), L-lysine ($C_6H_{14}N_2O_2$, PR), sodium carbonate (Na_2CO_3, 99.0%), ethylene glycol ($C_2H_6O_2$, ≥ 99.5%), sodium hydroxide (NaOH, ≥ 96.0%), ethanol (C_2H_6O, 99.5%) and potassium nitrate (KNO_3, ≥ 99.0%) were purchased from Sinopharm Chemical Reagent. Ammonium chloride (NH_4Cl, PT), salicylic acid ($C_6H_4(OH)COOH$, ≥ 99.0%) and sodium hypochlorite solution (NaClO, available chlorine ≥ 5.0%) were purchased from Aladdin Reagent. Sodium nitroferricyanide (III) dihydrate ($Na_2[Fe(CN)_5NO]·2H_2O$, 99.0%), potassium nitrite (KNO_2, 97%), sulfanilamide ($C_6H_8N_2O_2S$, 99.5%), N-(1-Naphthyl) ethylenediamine dihydrochloride ($C_{12}H_{14}N_2·2HCl$, > 98.0%) and potassium hydroxide (KOH, 99.99%) were obtained from Macklin. Dimethyl sulfoxide-d6 (DMSO-d6, (D, 99.9%) + 0.03% V/V TMS) was obtained from Cambridge Isotope Laboratories. Deionized (DI) water with a resistivity of 18.2 MΩ·cm was used in all experiments.

Synthesis of the Cu/CoCH NSs. In a typical synthesis, 2 mmol $Co(NO_3)_2·6H_2O$, 1 mmol $Cu(NO_3)_2·3H_2O$ and 0.438 g L-lysine were added into 15 mL DI water and 15 mL ethylene glycol , and stirred for 30 min at room temperature. Next, 3 mL 1.2 M Na_2CO_3 was added to the solution under magnetic stirring and maintained for 60 min. After that, the prepared solution was sealed into a 100 mL Teflon-liner stainless steel autoclave and placed into an oven at 180 °C for 5 h to prepare Cu/CoCH NSs. After cooling down to room temperature, ethanol was added to the solution and purified, then redispersed in ethanol. The Cu/CoCH NSs catalysts were controlled by changing the adding amount of $Co(NO_3)_2·6H_2O$ and $Cu(NO_3)_2·3H_2O$ to 1.5 mmol. The synthesis of pure CoCH NSs was similar to that of Cu/CoCH NSs with the only difference being that without adding $Cu(NO_3)_2·6H_2O$. Cu/CoCH NSs with different feeding molar ratio of Co to Cu were prepared by changing the adding amount of $Cu(NO_3)_2$ during the synthesis process, including 4:1, 2:1, 1:1 and 1:2, named a-Cu/CoCH, b-Cu/CoCH, c-Cu/CoCH NSs and c-Cu/CoCH NSs.

Synthesis of the Cu-CoO NSs. The Cu/CoCH NSs precursor was transformed into Cu-CoO NSs through calcination at 400°C for 2 h with a heating rate of 1 °C min^{-1} under Ar flow. Cu-CoO NSs catalysts with different feeding molar ratio of Co to Cu were named a-Cu-CoO, b-Cu-CoO, c-Cu-CoO and d-Cu-CoO NSs, respectively. According to inductively coupled plasma optical emission spectrometry (ICP-OES) measurements, the mass ratio of Cu to Co in b-Cu-CoO NSs is 1:2.

Synthesis of the Cu-Co_3O_4 NSs. The Cu/CoCH NSs precursor was transformed into Cu-Co_3O_4 NSs through calcination at 300°C for 4 h with a heating rate of 1 °C min^{-1} under air flow. The synthesis of pure Co_3O_4 NSs was similar to that of Cu-Co_3O_4 NSs with the only difference being that without adding $Cu(NO_3)_2 \cdot 6H_2O$.

Synthesis of the Cu nanoparticles (NPs). The pure Cu NPs were synthesized by adding 1 mL 0.1 M $CuCl_2$ and 1 mL 0.2 M NaOH into 30 mL DI water and 1 mL ethanol under magnetic stirring. Then adding 5 mL 10 mg/mL $NaBH_4$ to solution under Ar flow. The products were washed by DI water and ethanol.

NO_3RR performance evaluations. The electrochemical measurements were carried out in a customized gastight two-compartment H-cell, that was composed of an anodic chamber and a cathodic chamber, separated by a Nafion 211 membrane. Each chamber was loaded with 30 mL KOH (1 M) /KNO_3 (0.1 M) aqueous solution as both the cathodic and anodic electrolyte. All measurements were employed using a potentiostat (CHI 660E) equipped with a typical three-electrode system at room temperature. A graphite rod and an Ag/AgCl (filled with saturated KCl solution) electrode were used as reference and counter electrodes, respectively. The working electrode was obtained by dispersing the catalyst in a mixture of 100 μL ethanol and 10 μL Nafion solution (5 wt%) under ultrasonication for 10 min. 20 μL of this suspension was deposited onto a glassy carbon plate in an area of 1 cm^2 (1 cm × 0.5 cm × 2) and allowed to dry under ambient conditions to achieve a catalysts mass loading of ~1 mg cm^{-2}. The potentiostatic tests was conducted at constant potentials for 0.5 h at a stirring rate of 400 rpm. All potentials were converted to the RHE scale by E (vs RHE) = E (vs Ag/AgCl) + 0.197 V + 0.0591 × PH. The LSV curves were obtained by scanning the potential from −0.1 to −0.6 V vs RHE at a rate of 5 mV s^{-1}.

Determination of NH_3 concentration using the indophenol blue method. The concentration of produced NH_3 was spectrophotometrically determined by the indophenol blue method with modification.[1] First, 0.5 mL NO_3RR electrolyte was removed from the electrochemical reaction cell, mixed with 0.5 mL HCl (1 M) aqueous solution and diluted to the detection range. Then, 2 mL of solution was removed from the diluted electrolyte. Subsequently, the remaining solution (0.5 mL), salicylic acid (1 M in 1.17 M NaOH solution, 0.4 mL), sodium nitroprusside (0.1 g in 10 mL water, 0.025 mL), and NaClO (available chlorine content 0.35 wt% in 0.7 M NaOH, 0.025 mL) were sequentially added into DI water (1.55 mL). After 1.5 h at room temperature, the absorption spectrum was measured by using a UV–vis spectrophotometer. The formation of indophenol blue was determined at a wavelength of 685 nm. The concentration–absorbance calibration curve was obtained by using various standard NH_4Cl solutions.

Determination of NH_3 concentration using the ^1H NMR spectroscopy. To support the UV-vis results, the amount of produced $^{14}NH_3$ and $^{15}NH_3$ were also quantified by the ^1H NMR spectroscopy. DMSO-d6 and maleic acid ($C_4H_4O_4$) were used as solvent and the internal standard.[2] The calibration curve was achieved using the peak area ratio between NH_4^+ and $C_4H_4O_4$. 0.1 mL post-NO_3^-RR electrolyte was removed from the electrochemical reaction cell and mixed with 0.11 mL HCl (1 M) aqueous solution, then 10 μL maleic acid (32 mM) and 280 μL DMSO-d6 were added. The produced NH_4^+ concentration can be calculated from the peak area using the calibration curve.

Determination of NO_2^- concentration using colorimetric method. After chronoamperometry tests, NO_2^- in electrolyte was determined by reported colorimetric method with modification.[3] First, 0.25 g of sulfanilamide was dissolved in 20 mL of 2 M HCl solution (regent A), 20 mg of N-(1-Naphthyl) ethylenediamine dihydrochloride was dissolved in 20 mL of DI water (regent B). Next, 0.5 mL of electrolyte was taken out from the electrolytic cell, mixed with 0.5 mL 1 M HCl and diluted to the detection range. Then 1 mL diluted solutions was extracted and mixed with 3.8 mL DI water. 0.1 mL regent A and 0.1 mL regent B were sequentially added into the above solution. The solution was mixed uniformly and then left undisturbed at room temperature for 0.5 h to allow for the complete color development. The absorption spectrum was measured by using a UV–vis spectrophotometer, and the absorption intensity was recorded at a wavelength of 540 nm.

Determination of NO_3^- concentration. NO_3^- in electrolyte was determined by reported colorimetric method with modification.[4] A certain amount of electrolyte was taken out from the electrolytic cell and diluted to 5 mL to detection range. Then, 0.1 mL 1 M HCl and 0.01 mL 0.8 wt% sulfamic acid solution were added into the aforementioned solution. The absorption spectrum was measured using an UV-Vis spectrophotometer and the absorption intensities at a wavelength of 220 was recorded. The concentration-absorbance curve was calibrated using a series of standard potassium nitrate solutions.

Determination of N_2H_4 concentration. N_2H_4 in the electrolyte was determined by the Watt and Chrisp method.[5] Typically, 5.99 g of 4-(dimethylamino)benzaldehyde, 30 mL of hydrochloric acid and 300 mL of ethanol were thoroughly mixed and used as a color reagent. Then, 2.5 mL of electrolyte were collected from the cathode compartment and mixed with 2.5 mL of the above color reagent. After standing in the dark for about 20 mins at room temperature, the absorbance of the obtained solution was measured at a wavelength of 457 nm by using the UV-vis spectrophotometer. The concentration-absorbance curve was made using standard hydrazine monohydrate solutions with a series of known concentrations.

Kinetic evaluation. The rate constants of electrochemical NO_3^- reduction (k_1) and electrochemical NO_2^- reduction (k_2) were conducted at − 0.4 V versus RHE in 1 M KOH + 0.1 M KNO_3 or 0.1 M KNO_2, respectively. Supposing that the concentrations of NO_3^- or NO_2^- declined exponentially as per the first-order rate, the rate constants (k_1 or k_2) were calculated by plotting the concentration of NO_3^- or NO_2^- against the time of reaction.

$$C_t = C_0 \exp(-k \times t)$$

while C_0 is the initial concentration of NO_3^- or NO_2^- (g mL^{-1}), C_0 refers to the concentration of NO_3^- or NO_2^- at time t (g mL^{-1}), and t is the time of reaction (min).

NO_3^- adsorption. In order to test the adsorption capacity of the catalysts (Cu NPs, CoO NSs and Cu-CoO NSs) for nitrate, the catalyst with an area of 1*1 cm^2 was immersed in 5 mL, 0.1 mol L^{-1} nitrate solution. After conducting 200 cycles of CV testing in the no-Faradaic range, the nitrate content in the electrolyte was detected.

Electrochemically active surface area (ECSA) evaluation. For ECSA estimation, the double-layer capacitance (C_{dl}) was assessed through cyclic voltammetry (CV) in a non-Faradaic potential region using various scan rates (20, 30, 40, 50, 60, 80, and 100 mV s^{-1}) in an electrolyte solution composed of 1 M KOH + 0.1 M KNO_3. The double-layer capacitance was extracted from the linear correlation between the current density (measured at a fixed potential within the non-Faradaic window) and the scan rate, where the slope of this linear plot corresponds to the C_{dl} value. Chronoamperometry tests for NO_3RR were conducted at different applied potentials for 1 h duration.

DFT calculations. All the DFT calculations were conducted based on the Vienna Ab initio Simulation Package (VASP). The exchange-correlation potential was described by the Perdew−Burke−Ernzerhof (PBE) generalized gradient approach (GGA). The electron-ion interactions were accounted by the projector augmented wave (PAW). All DFT calculations were performed with a cut-off energy of 400 eV, and the 2×1×1 Gamma centered Monkhorst-Pack grids k-points were selected to sample the Brillouin zone integration. The energy and force convergence criteria of the self-consistent iteration were set to 10^{-5} eV and 0.05 eV $Å^{-1}$, respectively. DFT-D3 method was used to describe van der Waals (vdW) interactions .Adsorption energy (E_{ads}) was calculated by using the following definitions:

$$E_{ads} = E_{total} - E_{slab} - E_{adsorbate}$$

Where the Etotal is the total electronic energy for the adsorbate and slab; Eslab is the electronic energy of slab, Eadsobate is the electronic energy of the molecules.

Characterization. TEM imaging was conducted on an HT7700 electron microscope operated at 100 kV. HRTEM, HAADF-STEM imaging and EDX elemental mapping were carried out on an FEI Themis Z microscopy. XRD patterns were carried out on a Smart Lab Se diffractometer equipped with Cu Kα radiation. XPS spectra were obtained on a Thermo Scientific ESCALAB 250Xi spectrometer equipped with an Al Kα X-ray source (hν = 1486.6 eV). All XPS spectra were calibrated using the C 1s peak at 284.8 eV to eliminate the influence of sample charging and instrumental deviation. ^{1}H NMR spectra were measured on a Bruker Avance III HD 600 NMR spectrometer. Electron paramagnetic resonance (EPR) spectroscopy was tested on Bruker EMXnano. N_2 adsorption–desorption isotherms were recorded on an PM7500 Series accelerated surface area and porosimetry instrument (Huapu Hengchuang Instrument Technology), equipped with automated surface area using Barrett–Emmett–Teller calculations. The extinction spectra were obtained by a Hitachi U-3900 ultraviolet/visible/NIR spectrophotometer. The gaseous products were quantitatively detected by an off-line gas chromatograph (GC, Agilent Technologies 7890B). ICP-OES was measured on a PerkinElmer Optima 7300 DV system.

Supporting Figures

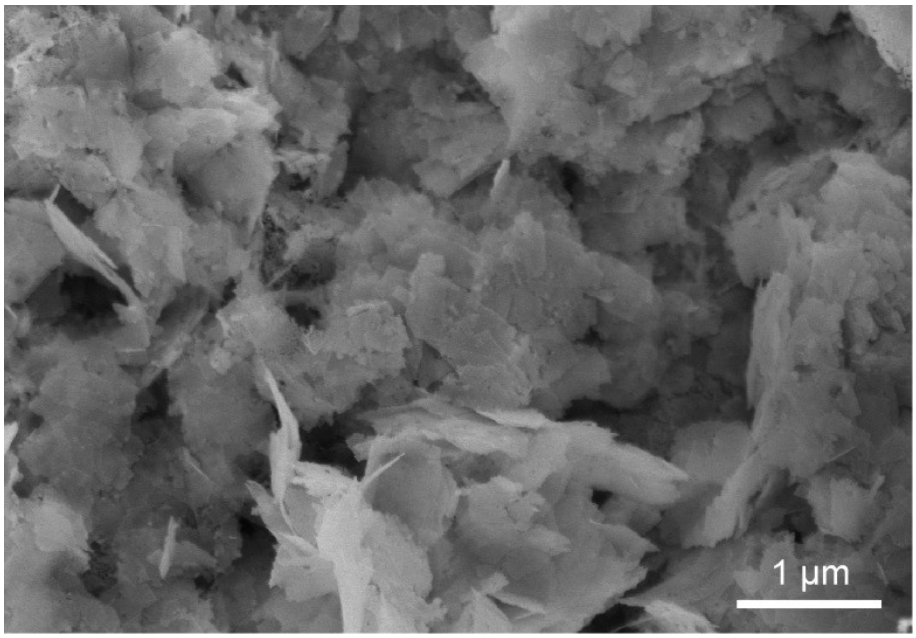

Figure S1. Representative SEM image of the Cu-CoO NSs at a low magnification.

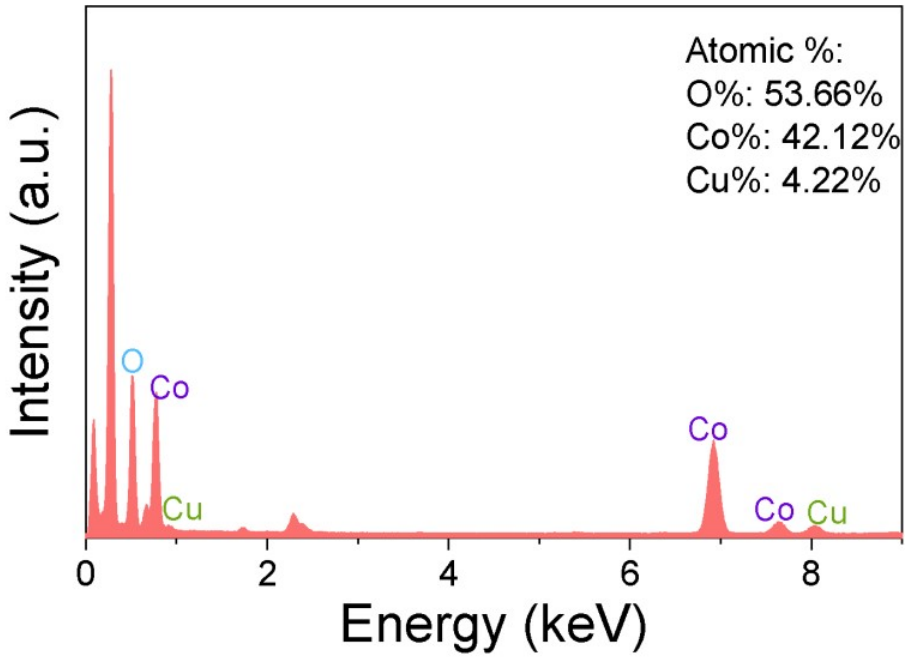

Figure S2. EDX spectrum of Cu-CoO NS.

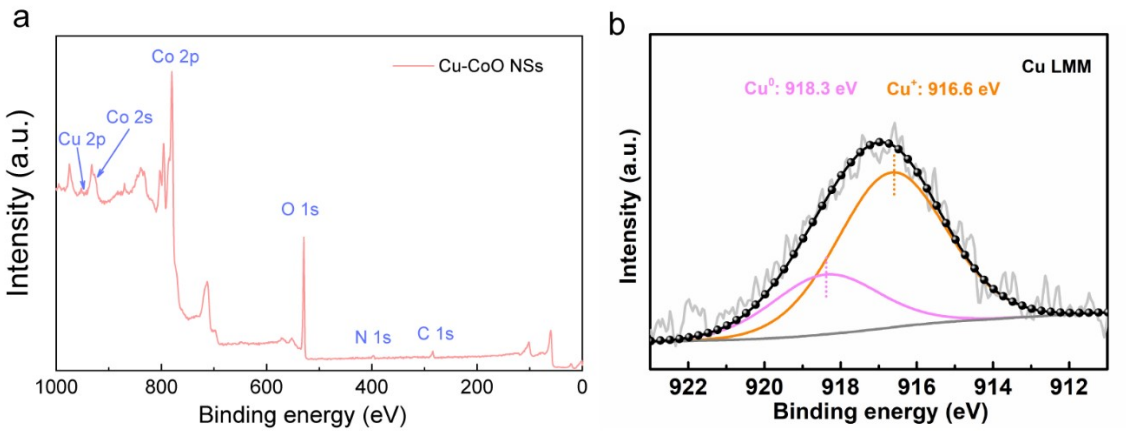

Figure S3. XPS survey spectrum (a) and Cu LMM spectra (b) of the Cu-CoO NSs.

As shown in Figure S3b, the Cu LMM Auger spectrum is further used to distinguish the metallic Cu and Cu^+ ions. Specifcally, the peak located at 918.3 eV indicates the existence of Cu^0, while a broad kinetic energy at 916.6 eV indicates the existence of Cu^+.[6]

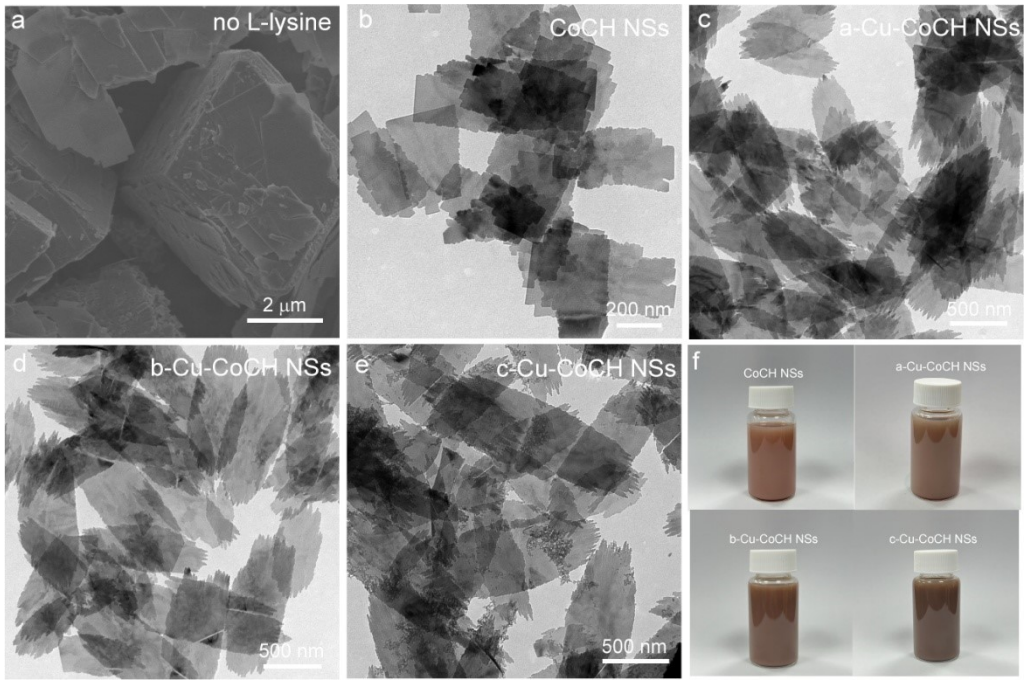

Figure S4. (a) The TEM image of Cu/CoCH products without adding L-lysine. (b–f) The TEM images of Cu/CoCH products with different Co:Cu feeding molar ratio, including CoCH (b), a-CoCH (c), b-CoCH (d) and c-CoCH (e). (f) The photographs of the corresponding colloidal solutions of different Cu/CoCH products.

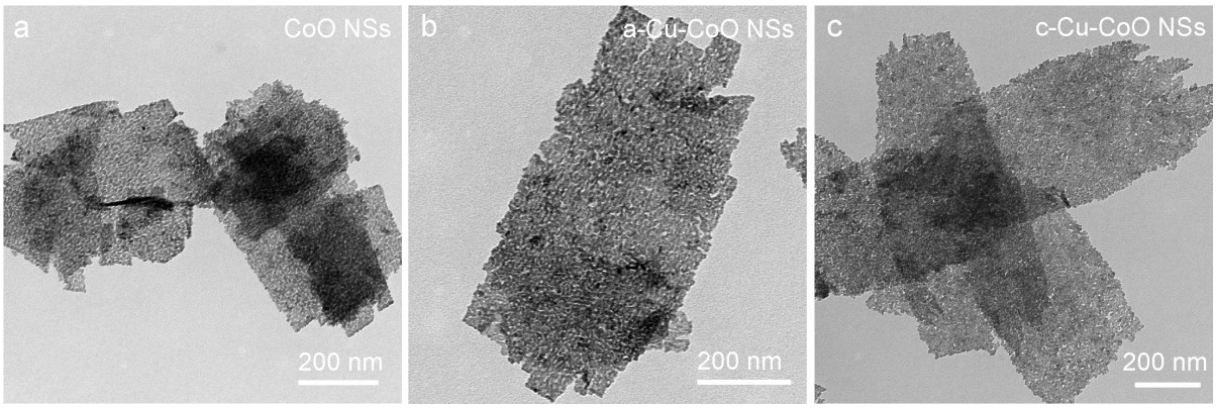

Figure S5. TEM images of CoO NSs (a), a-Cu-CoO (b) and c-Cu-CoO NSs (c).

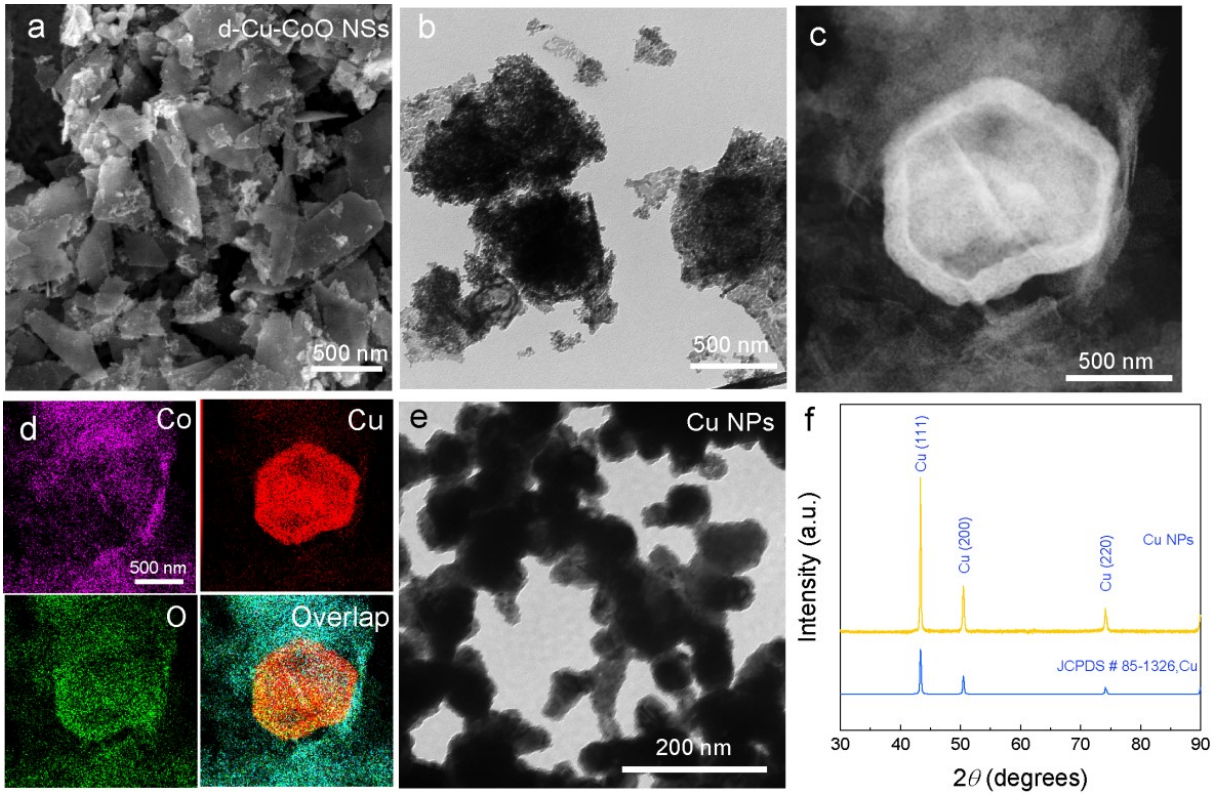

Figure S6. (a-d) SEM (a),TEM (b), HAADF-STEM image (c) and the corresponding elemental maps (d) of d-Cu-CoO NSs. (e, f) TEM image (e) and XRD spectrum (f) of Cu NPs.

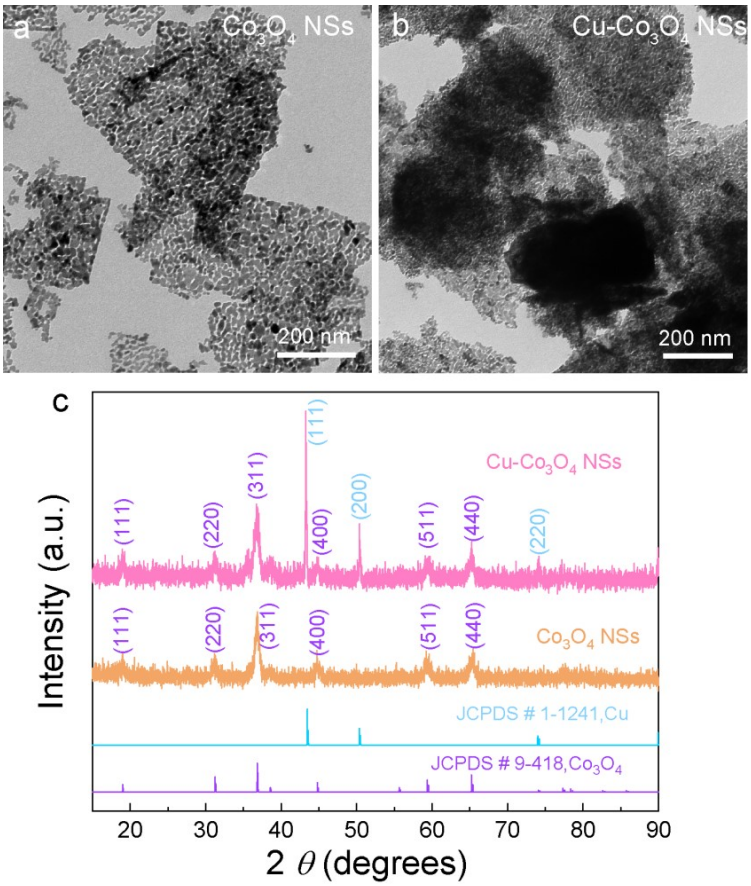

Figure S7. (a, b) TEM images of Co_3O_4 NSs (a) and Cu-Co_3O_4 NSs (b). (c) XRD spectrum of the Co_3O_4 NSs and Cu-Co_3O_4 NSs.

As shown in Figure S7d, to clarify the Cu oxidation state in Cu-Co_3O_4 NSs, the Cu LMM Auger spectrum Cu-Co_3O_4 NSs is further used to distinguish the metallic Cu and Cu^{2+} ions. Specifcally, the peak located at 918.3 eV indicates the existence of Cu^0 , while a broad kinetic energy at 916.6 eV indicates the existence of Cu^+.[6] The result show that Cu exists in the metallic (0) and +1 oxidation states.

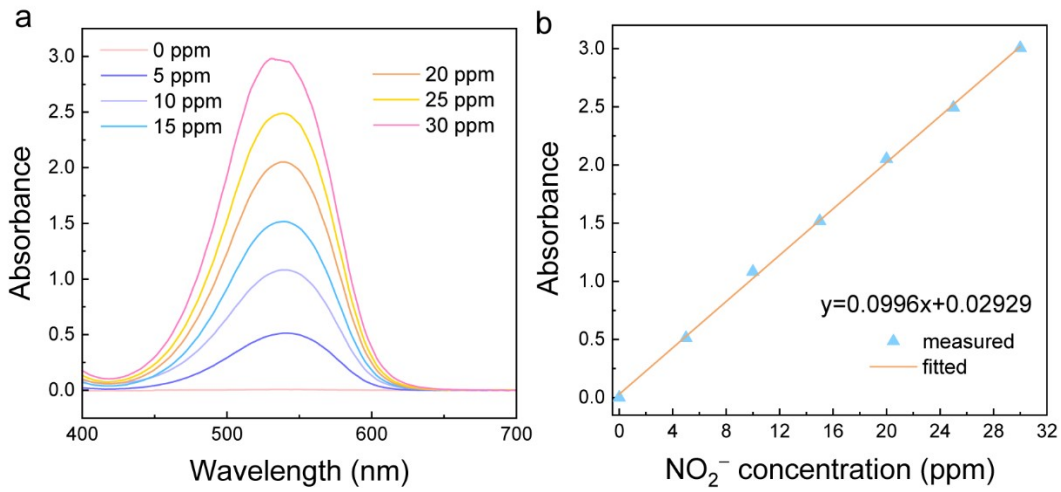

Figure S8. Calibration curve for the NO_2^-. (a) Absorption spectra of the standard KNO_2 solutions with different concentrations. (b) Linear relationship between the absorbance values and the concentrations of standard KNO_2 solutions. The coefficient of determination for the linear fitting is $R^2 = 0.99963$.

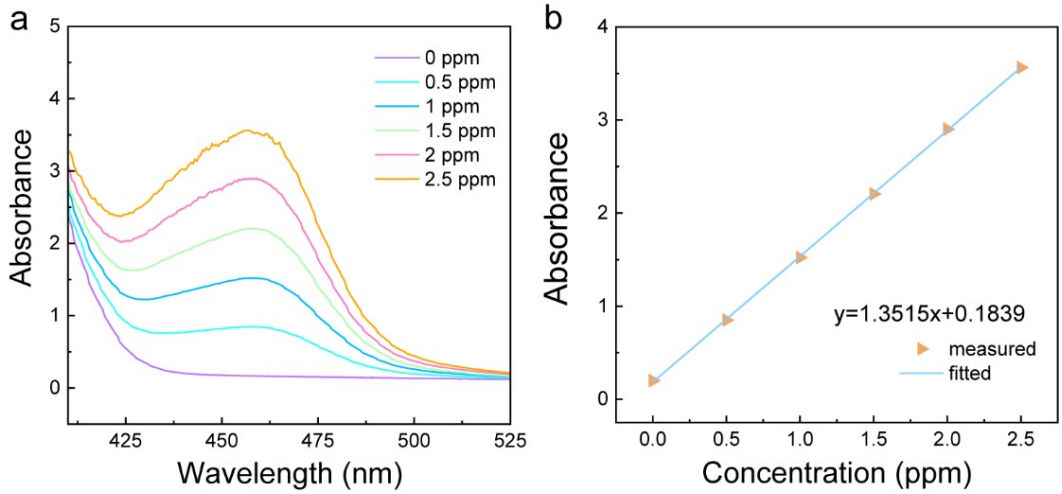

Figure S9. Calibration curve for the N_2H_4 detection method. (a) Absorption spectra of the standard N_2H_4 solutions with different concentrations. (b) Linear relationship between the absorbance values and the concentrations of standard N_2H_4 solutions. The coefficient of determination for the linear fitting is $R^2 = 0.9998$.

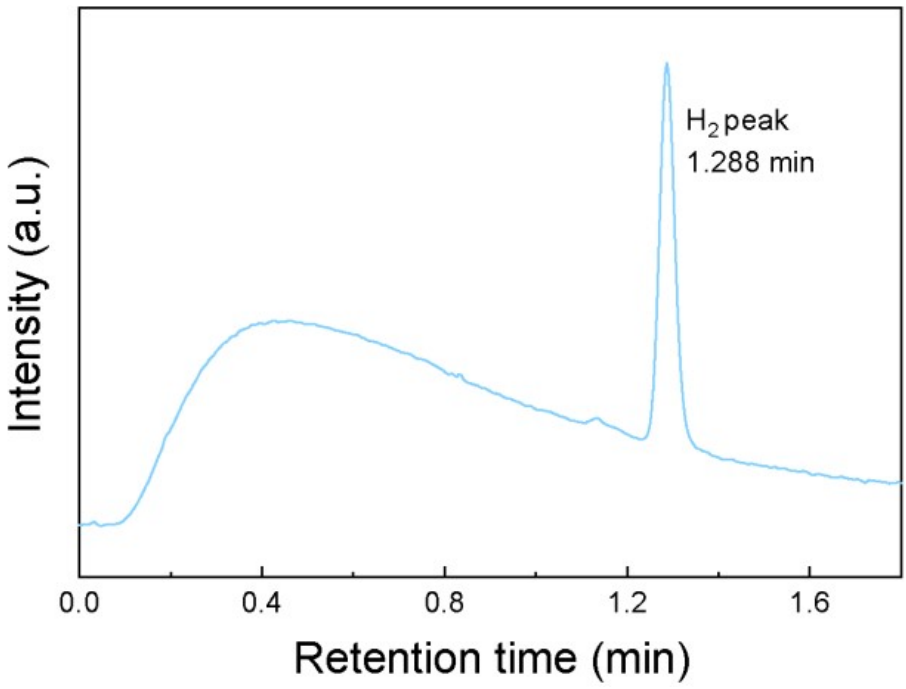

Figure S10. Detection of the possible H_2 evolution in the electrocatalytic process by GC.

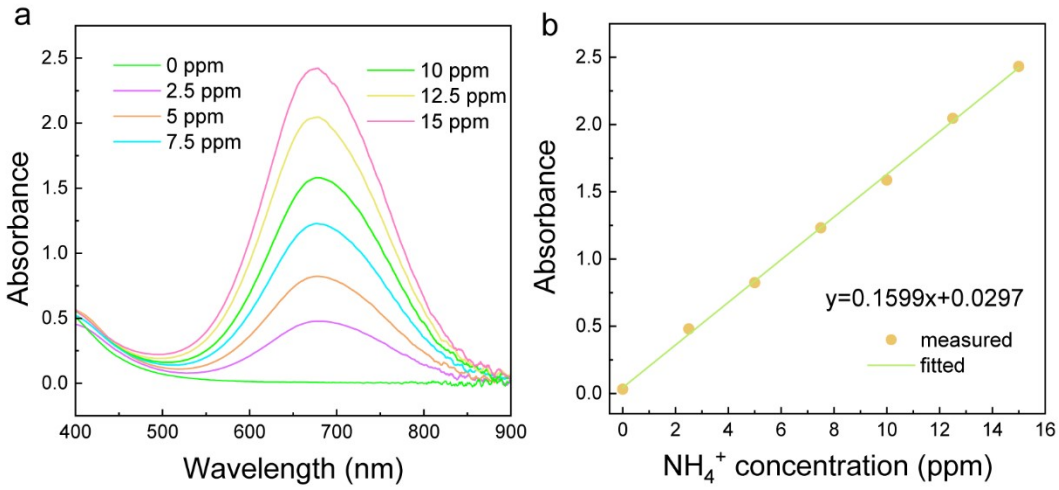

Figure S11. Calibration curve for the indophenol-blue method. (a) Absorption spectra of the standard NH_4Cl solutions with different concentrations. (b) Linear relationship between the absorbance values of the formed indophenol blue and the concentrations of standard NH_4Cl solutions. The coefficient of determination for the linear fitting is $R^2 = 0.9991$.

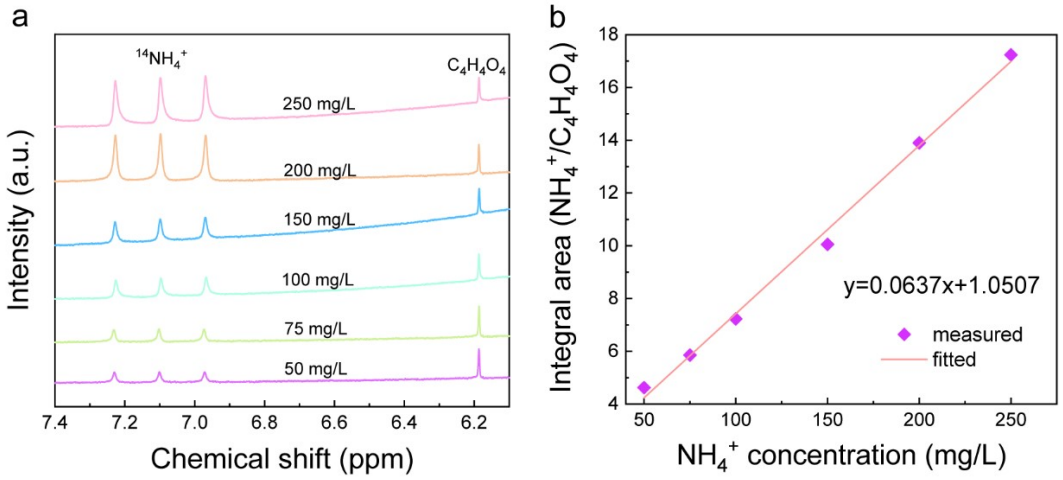

Figure S12. Calibration curve for ^{1}H NMR spectra. (a) ^{1}H NMR spectra of the standard $^{14}NH_4Cl$ solutions with different concentrations using maleic acid as an internal standard. (b) Linear relationship between the integrated peak areas and the standard $^{14}NH_4^+$ solution concentrations. The coefficient of determination for the linear fitting is $R^2 = 0.9952$.

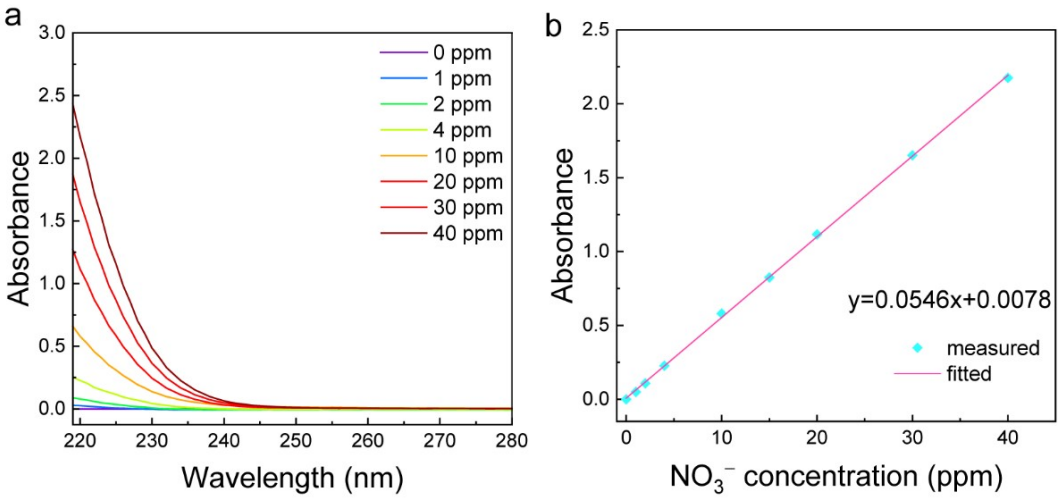

Figure S13. Calibration curve for the NO_3^- detection method. (a) Absorption spectra of the standard NO_3^- solutions with different concentrations. (b) Linear relationship between the absorbance values and the concentrations of standard NO_3^- solutions. The coefficient of determination for the linear fitting is $R^2 = 0.9996$.

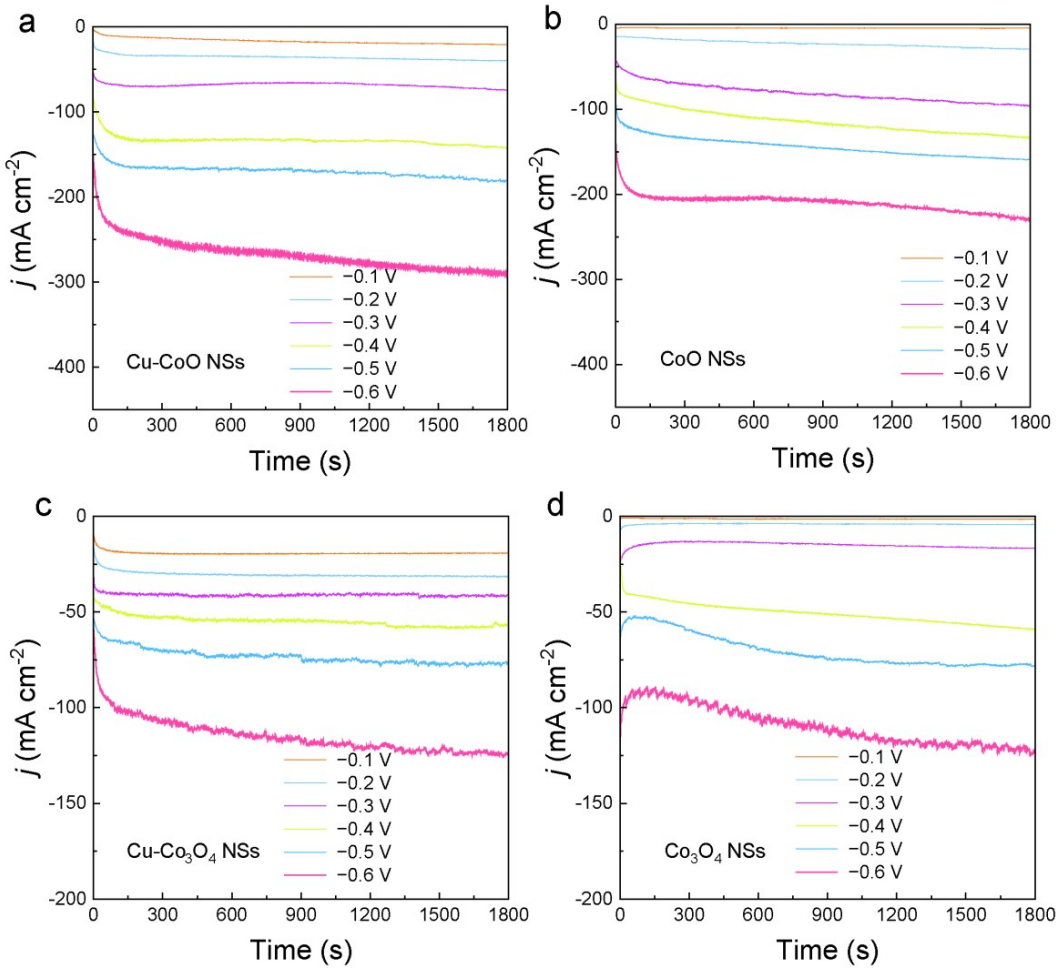

Figure S14. Chronoamperometry curves of Cu-CoO (a), CoO (b), Cu-Co_3O_4 (c) and Co_3O_4 (d) electrocatalysts after 0.5 h electrolysis of NO_3RR.

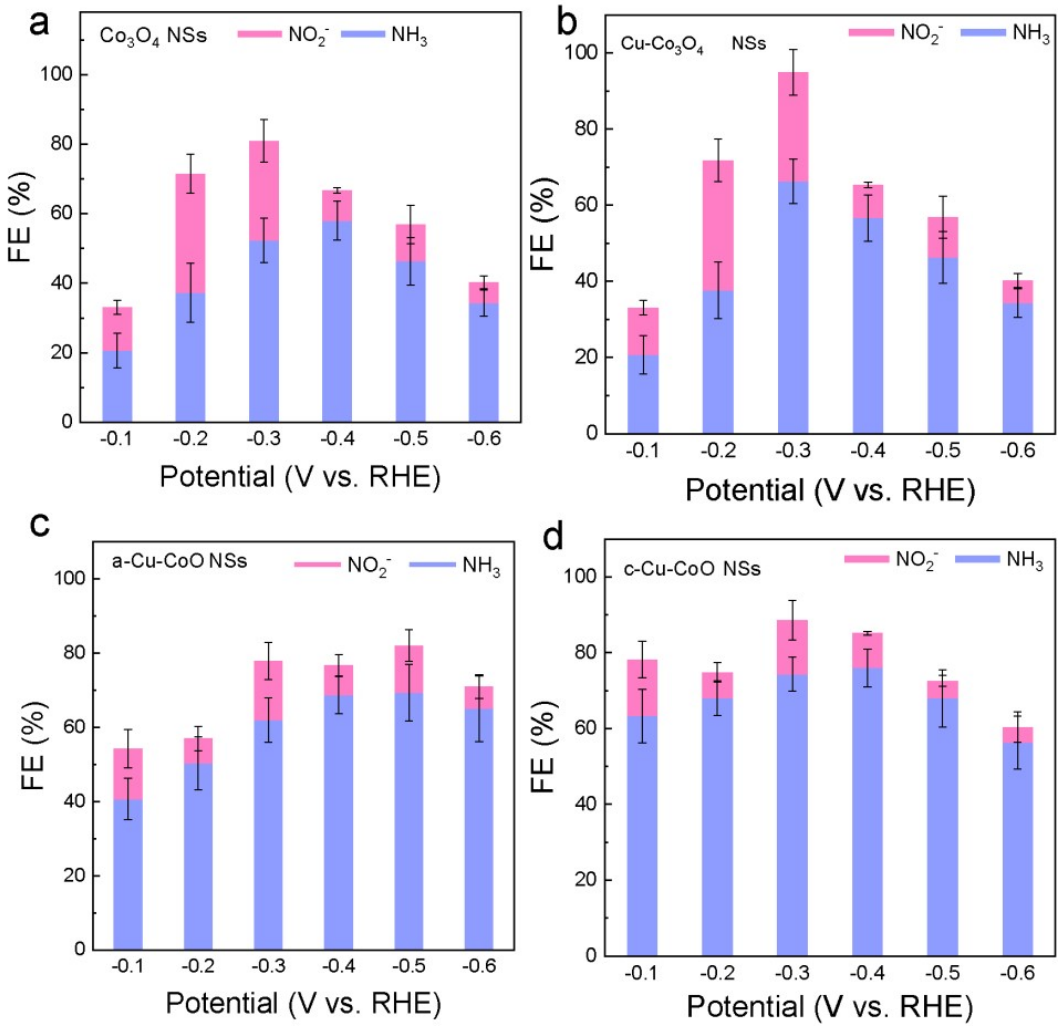

Figure S15. FEs of different products obtained by using Co_3O_4 NSs (a), Cu-Co_3O_4 NSs (b), a-Cu-CoO NSs (c) and c-Cu-CoO NSs (d) electrocatalysts at different potentials.

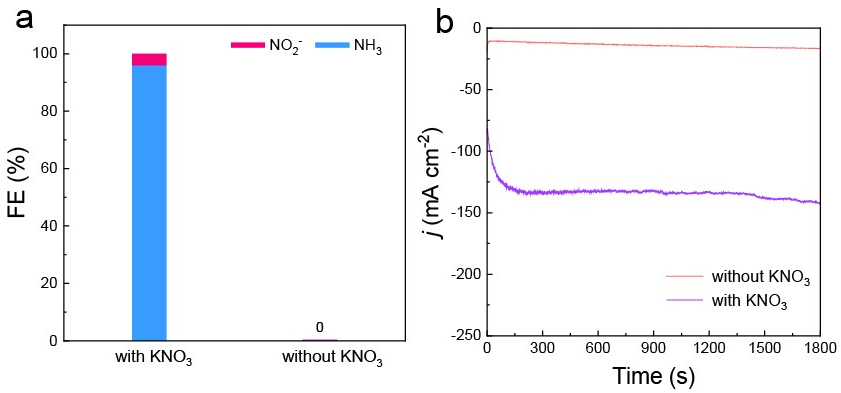

Figure S16. (a, b) FE of different products (a) and chronoamperometry curves (b) of Cu-CoO NSs in 1 M KOH solution with or without NO_3^- at –0.4 V vs. RHE.

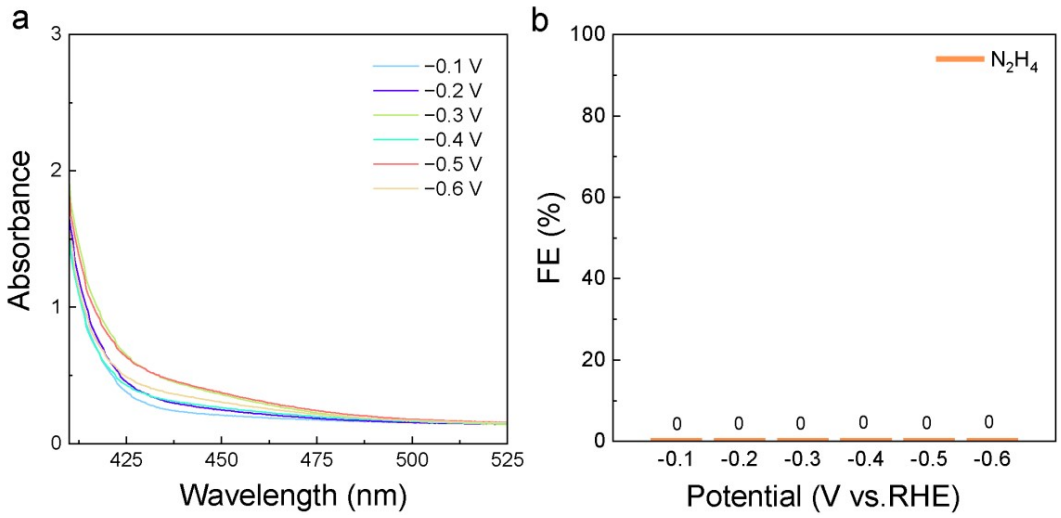

Figure S17. Absorption spectra (a) and FEs (b) of N_2H_4 products obtained by using Cu-CoO NSs electrocatalysts at different potentials.

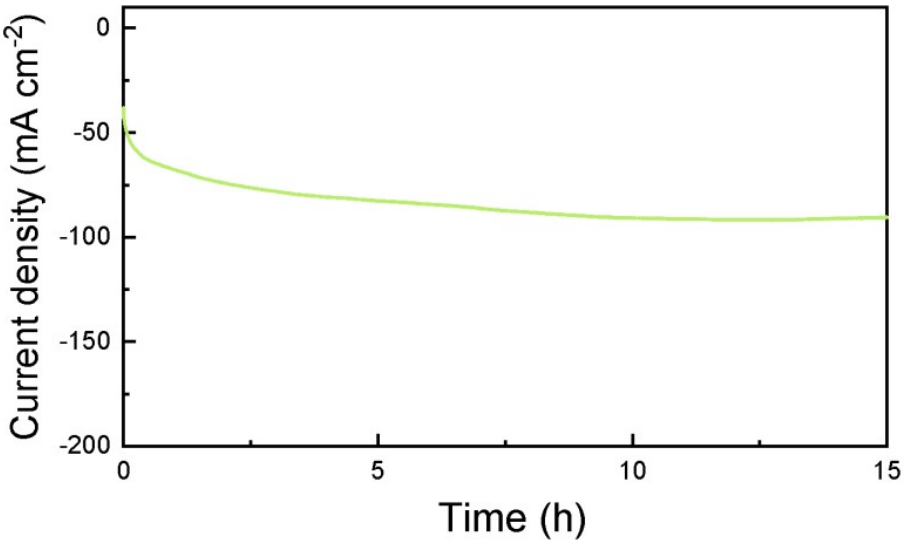

Figure S18. Stability test. Long-term chronoamperometry test for 15 h at − 0.4 V on the Cu-CoO NSs.

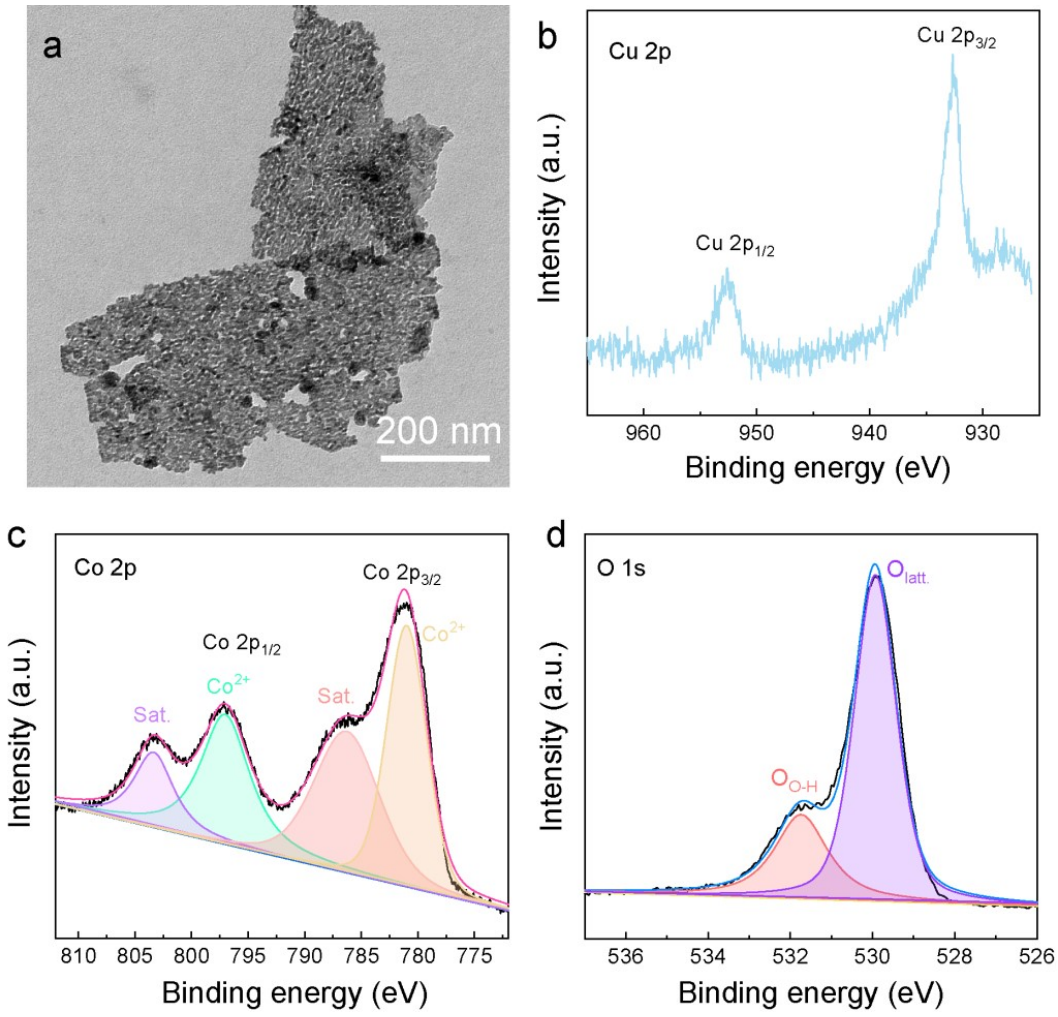

Figure S19. Stability test. (a−d) TEM image (a), high-resolution Cu 2p spectra (b), high-resolution Co 2p spectra (c) and high-resolution O 1s (d) spectra of the Cu-CoO NSs after the electrocatalytic process.

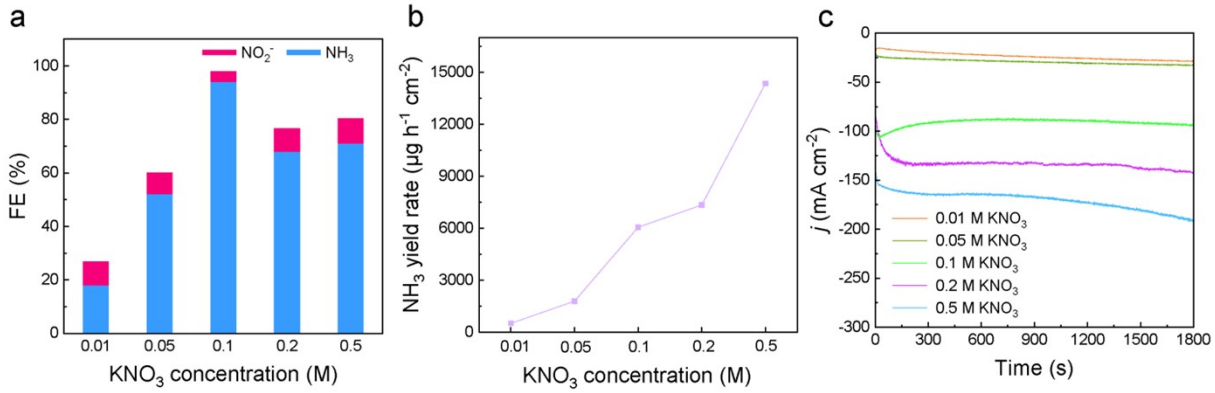

Figure S20. Effect of the KNO_3 concentrations on NO_3RR. (a–c) FEs of different products (a), NH_3 yield rate (b) and *i*–*t* curves (c) of NO_3^- reduction on Cu-CoO NSs at different concentrations of KNO_3 at –0.4 V vs. RHE.

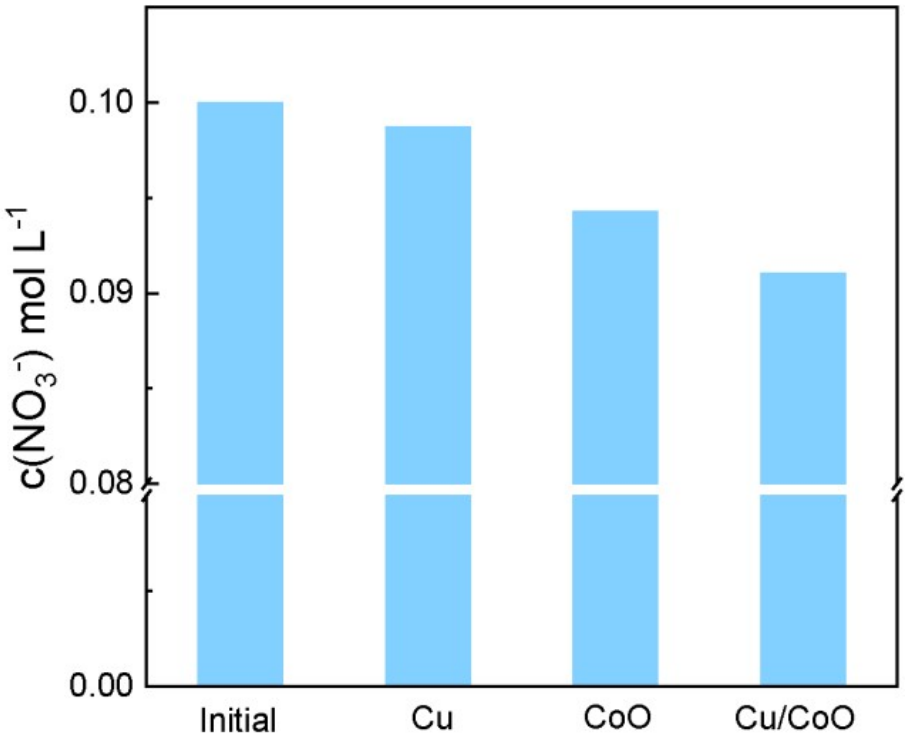

Figure S21. Adsorption capacity test. The concentration of nitrate in the electrolyte after the adsorption by Cu NPs, CoO NSs and Cu-CoO NSs.

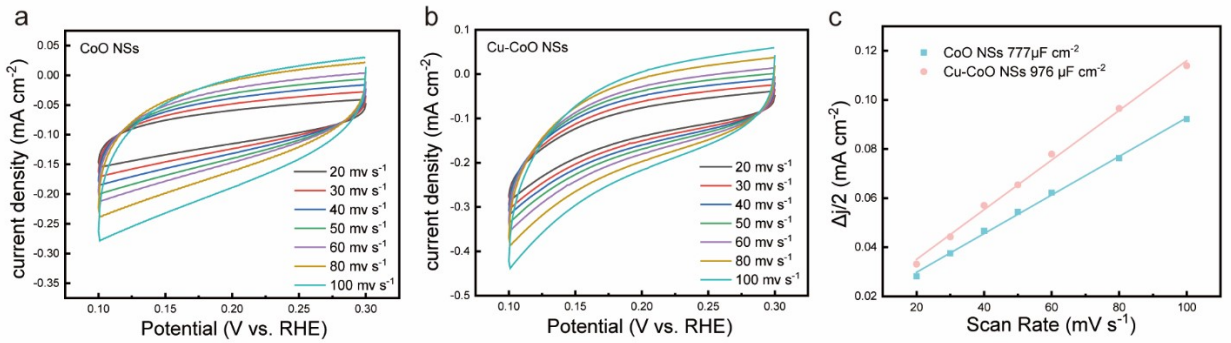

Figure S22. (a, b) Cyclic voltammograms (CV) are used to determine the double−layer capacitance of (a) CoO NSs and (b) Cu-CoO NSs in 1 M KOH and 0.1 M KNO_3. (c) Plots of the current densities against CV scan rates. The slopes observed in the plots positively correlate with the electrochemical double-layer capacitance (C_{dl}) per geometric area of the electrode and also demonstrate a correlation with the ECSA.

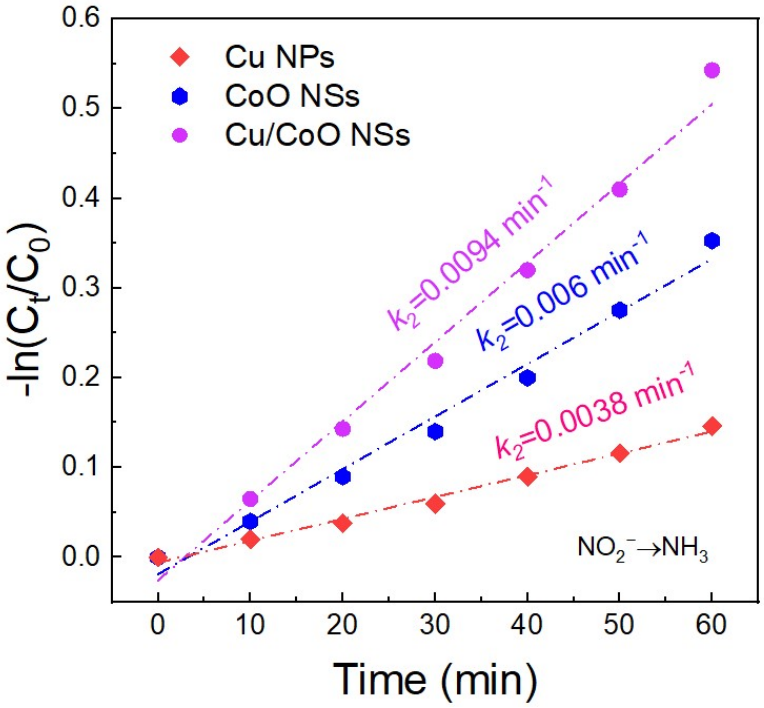

Figure S23. Electrochemical kinetic analysis. Linearized pseudo first-order kinetic profiles of Cu, CoO and Cu-CoO NSs in 1 M KOH + 0.1 M KNO_2, respectively.

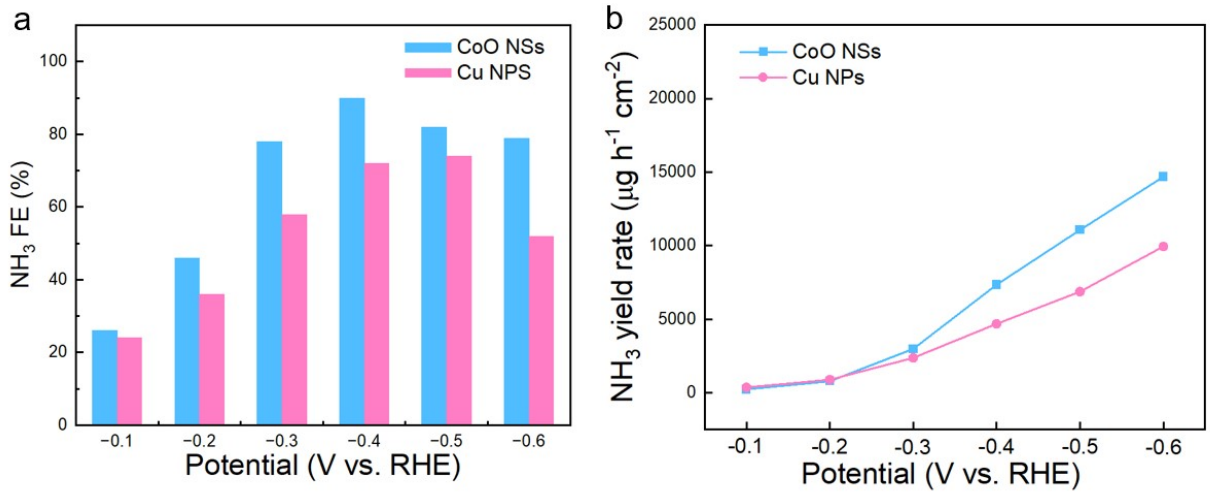

Figure S24. FEs of NH_3 products (a) and NH_3 yield rate (b) obtained by using CoO NSs and Cu NPs electrocatalysts at different potentials.

Supporting Tables

Table S1. Summary of NH_3 product FE values in recently reported Cu-based electrocatalysts.

Catalyst	Electrolytes	Yield rate / μg h^{-1} cm^{-2}	FE / %	Ref.
Cu-CoO NSs	1 M KOH + 0.1 M KNO_3	13668	94.7	this work
CuNiFe-LDH HNCs	0.05 M Na_2SO_4 + 0.05 M $NaNO_3$	3580	90.1	7
Cu1/Cl-CeO_2@C	0.1 M KNO_3 + 0.5 M KOH	9528	98.8	8
P-$Cu_{0.51}Ni_{0.49}$	0.5 M K_2SO_4 and 50 ppm KNO_3	1616.94	98.38	9
Cu-CoP	0.1 M K_2SO_4 + 10 mM KNO_3	7650	85.1	10
HEA	1 M KOH + 0.5 M KNO_3	3250	92	11
FeCu-NC	0.1 M KOH + 0.1 M KNO_3	6130	95	12
$Cu(OH)_2$ NWs	0.5 M K_2SO_4 + 200 ppm KNO_3	7853	96.8	13
Ni_1Cu	1 M KOH + 0.1 M KNO_3	9700	80	14

References

1. J. H. Yang, Y. Z. Guo, R. B. Jiang, F. Qin, H. Zhang, W. Z. Lu, J. F. Wang, J. C. Yu, *J. Am. Chem. Soc.* 2018, **140**, 8497−8508.
2. M. H. Xie, S. S. Tang, Z. Li, M. Y. Wang, Z. Y. Jin, P. P. Li, X. Zhan, H. Zhou, G. H. Yu, *J. Am. Chem. Soc.* 2023, **145**, 13957−13967.
3. L. Q. Li, C. Tang, D. Z. Yao, Y. Zheng, S. Z. Qiao, *ACS Energy Lett.* 2019, **4**, 2111−2116.
4. W. Q. Yu, J. Y. Yu, M. Huang, Y. J. Wang, Y. J. Wang, J. W Li, H. Liu and W. J. Zhou, ***Energy Environ. Sci.***, 2023, **16**, 2991-3001.
5. Y. H. Wang, Y. C. Xiong, M. Z. Sun, J. W. Zhou, F. K. Hao, Q. H. Zhang, C. L. Ye, X. X. Wang, Z. H. Xu, Q. B. Wa, F. Liu, X. Meng, J. Wang, P. Y. Lu, Y. B. Ma, J. W. Yin, Y. Zhu, S. Q. Chu, B. L. Huang, L. Gu, Z. X. Fan, *Angew. Chem. Int. Ed.* 2024, **63**, e202402841.
6. W. F. Liu, Z. Zhang, Y. N. Zhang, Y. F. Zheng, N. S. Liu, J. Su and Y. H. Gao, *Nano-Micro Lett.* 2021, **13**, 61.
7. Y. L. Fu, Y. L. Li, F. Q. Fan, B. B. Chen, X. J. Hou, Y. H. Li, H. Li, Y. Fu, W. Qi, *ACS Catal.* 2025, **15**, 6918−6928.
8. S. Y. Wang, X. Ji, S. C. Wang, P. Jing, X. Xu, B. C. Liu, J. Zhang, *Adv. Funct. Mater.* 2025, **35**, 2502073.
9. S. L. Liu, Y. H. Cao, L. Yang, Y. H. Li, J. T. Li, B. W. Xin, G. G. Feng, H. Wang, C. Wang, *Small* 2025, **21**, 2500641.
10. W. H. Yang, Z. W. Chang, X. Yu, P. Wu, R. X. Shen, L. Z. Wang, X. Z. Cui, J. L. Shi, *Adv. Sci.* 2025, **12**, 2416386.
11. W. Y. Qiu, Y. Guo, X. Z. Fu, J. L. Luo, *Adv. Funct. Mater.* 2025, **35**, 2415970.
12. X. B. Meng, K. Wang, Z. Q. Zhao, K. Li, W. M. Sun, Y. Q. Lin, *Small* 2025, **21**, 2407216.
13. B. C. Zhang, Z. C. Dai, Y. X. Chen, M. Y. Cheng, H. K. Zhang, P. Y. Feng, B. Q. Ke, Y. Y. Zhang, G. Q. Zhang, *Nat. Commun.* 2024, **15**, 2816.
14. K. Liu, H. M. Li, M. H. Xie, P. F. Wang, Z. Y. Jin, Y. T. Liu, M. Zhou, P. P. Li, G. H. Yu, *J. Am. Chem. Soc.* 2024, **146**, 7779−7790.